2008

Umbrella-shaped gate field-effect transistor for biosensing measurements

Chengwu Tao
Iowa State University

Umbrella-shaped gate field-effective transistor for biosensing measurements

by

Chengwu Tao

A thesis submitted to the graduate faculty

in partial fulfillment of the requirements for the degree of

MASTER OF SCIENCE

Major: Electrical Engineering

Program of Study Committee:
Santosh Pandey, Major Professor
Liang Dong
Edward Yu

Iowa State University

Ames, Iowa

2008

TABLE OF CONTENS

LIST OF FIGURES

ABSTRACT

Based on previous CMOS-compatible biosensor designs and the flash memory technology, a novel Umbrella-Shaped Field-Effect Transistor (UGFET) is realized as a biochemical charge sensor in the MOSIS AMIS 1.5 um standard CMOS process. The devices show high scalability and versatility needed for VLSI application. The UGFET device architecture is modified from previous CvMOS (Shen et al. 2003) and CMFET (Barbaro et al. 2006) designs and is scaled down to maximize the charge sensing area and drastically improve the chip density. The device simulation results show an approximate 1 volt increase in floating gate voltage for every 10 nC/cm^2 charge density increase on the sensing electrode. The designed UGFET devices are quite stable and very sensitive to the gate potential change. Two methods based on shifts in the threshold voltage and drifts in the subthreshold voltage slope are developed to sense and detect miniscule charges in charged poly electrolytes and poly amino acids. All the measured results are consistent and show the applicability of using UGFET devices as charge-modulated biosensors. Array implemented sensor chips are also taped out and tested with biochemical solutions.

CHAPTER 1. INTRODUCTION

CMOS technology is attractive for its cheaper costs and well-established fabrication processes for a broad range of electronic applications. Therefore, fully CMOS-compatible biosensor devices are an attractive candidate for non-invasive biological experiments. By designing sensor devices that are compatible with standard fabrication processes without violating the sensitivity and stability requirements, CMOS-based biosensors will play an important role in biological detection and monitoring.

1.1 Objective

The goal of this work is to design a charge-modulated sensing device that can be fabricated in standard CMOS foundry and allows large scale integration as required in VLSI applications. Individual devices were to be designed on silicon chips for highly sensitive and repeatable charge sensing applications such as DNA hybridization or protein detection. VLSI components were also expected to be added on chip for fast addressing and readout of a large array of these devices.

1.2 Sensor technology and device

Based on previous CMOS-compatible sensor designs and with the inspiration of flash memory technique, a new sensor device is designed for improved scalability, fast readout and better reliability in a fully CMOS-compatible fabrication technology. The device consists of

an Umbrella-shaped Gate Field-Effect Transistor, which has significantly improved architecture compared to previous devices and requires no extra post layout processes.

1.3 Application

The designed UGFET devices adopt the merits of previous CMOS-compatible device (e.g. good sensitivity and stability), but shows better applicability as small-scale charge sensor in detecting biological processes. Various techniques were used to test the feasibility of applying UGFET devices for charge sensing, and a consistent test results convinced the further applicability in detecting charged molecules such as proteins and DNA strands. Array implemented sensor devices can be used to detect the charge fluctuation on a 2-D surface, thereby enabling a high density of these devices into arrays for real time monitoring and recording of cellular and other biological activities.

CHAPTER 2. PREVIOUS RESEARCH

Electrostatic processes between biochemical and solid state surface causes a deposition of biomolecules onto solid state surface. This deposition is widely applied in chemical coated biosensors such as DNA sensors ([Pedano et al., 2003], [Kim et al. 2004] and [Chiti et al., 2001]). Existing biosensors mostly utilize the property that specific proteins or DNA strands bind the chemicals with specific base or acids and thereby allow to sense optical or mechanical changes due to the molecule binding. These types of sensors are bulky, expensive and time consuming during measurements. Recently, new concepts of biosensing detects the solid surface potential variation (e.g. field effect transistors, capacitors) caused by the deposition of charged biomolecules such as proteins, DNAs and other charged biological molecules. Unlike established chemical or optical techniques, the new type of electronic biosensors are small in size, fast in detection, cheap in price, and compatible with CMOS fabrication technology.

2.1 Ion-Selective Field-Effect Transistor (ISFET)

A classic example of a biochemical sensor is the Ion Selective Field-Effective Transistor (ISFET) which was firstly realized in 1970. However, beyond the motivation of the ISFET technology, there were concerns with the electrical double layers created as the liquid-solid interface. For instance, measuring the action potentials caused by neural activity in experiments was always bothered by electrical and “biological” noise, and therefore much effort was made to detect local ion activities not affected by other double layers. Once the solid surface is immersed in the aqueous solution, charged molecules will be deposited at the solution-oxide or solution-nitride interface, as long as the silicon dioxide/nitride is

hydrophobic. This charged layer further interacts with the built-in double layers underneath at oxide-silicon junction, and forms a conducting channel in silicon in response to the molecular activity at the surface. This modifies the electronic drain current of the the ISFET device as shown in Figure 1 (Bergveld 1970). ISFET device with this sort of unique detection mechanism has inspired numerous chemical and biological sensing applications over several decades.

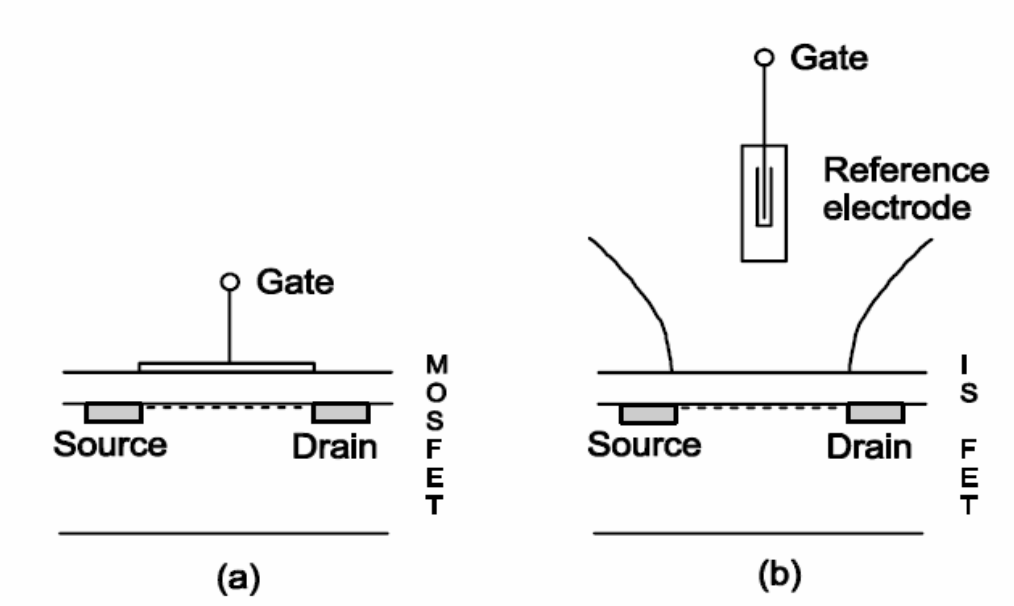

Figure 1. (a) Typical MOSFET cross sectional view, (b) ISFET cross sectional view.

A recent, exciting application of the ISFET technology is the EnFETs (enzyme-modified field-effect transistors). As shown in Figure 2, EnFET is based on pH variation sensing where the production or consumption of hydrogen ions in enzymatic reaction causes fluctuation of EnFET channel current. In practice, a different gate material or enzyme membrane immobilized on the sensing area will result in detection of specific biochemicals, such as glucose, urea, penicellin or organophosphorus (Schoning et al., 2006).

Based on the classical concept of pH sensing, the ISFET has been further applied in cellular measurements such as monitoring of electrical communication in neuron networks and measurements of ionic channels transportation (Schoning et al. 2006). Additionally, ISFET device-based sensor has been used to record the cellular acidificaiton and respiration rates by sensing the pH changes at the same site within a cell culture. A variation of several millivolts was detected in the sensing gate electrode during the activation of cells (Lehmann et al., 2001).

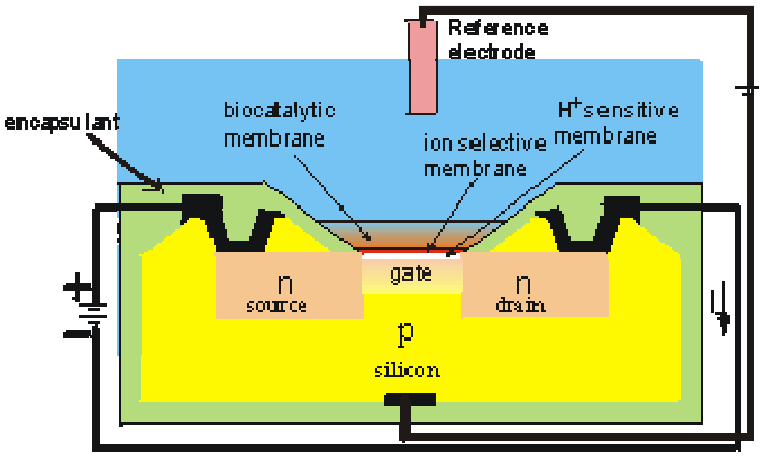

Figure 2. Enzyme modified FET.

ISFET technology very recently, has been demonstrated to detect DNA hybridization. Compared to standard methods such as radiochemical, enzymatic or fluorescent labels, ISFET sensors take advantage of an all-electronic scheme where the net charge fluctuation during the hybridization process is monitored at a faster rate. Specifically, during hybridization, charge associated with target molecule modulates the total charge on the sensing gate, and thereby changes the floating gate potential. The hybridization between ssDNA and pre-coated DNA strands causes the drain current to vary from tens of micro

amperes to hundreds of micro amperes, and hence allowing us to record the net current fluctuations due to hybridization (Schoning et al. 2006 and Kim et al. 2004).

The last decade has seen improvements in the ISFET technology with promising sensor applications in experiments requiring high sensitivity and selectivity. In biological applications such as detection of enzyme's cellular activities, DNA hybridization, and protein analysis, ISFET devices show easier experimental operation than traditional methods. They are also attractive for their portability, robustness, smaller size, fast detection, cheaper cost, and easier fabrication. Significant improvements in the ISFET device over other electronic sensors has been achieved by replacing the external reference electrode of conventional ISFETs by the capacitively coupled MOSFET gate (Schoning et al. 2006), which has been shown to be more convenient and miniaturized for experiments.

However, some disadvantages still limit the popularity of ISFET devices. Firstly, ISFET device fabrication needs special post fabrication steps beyond what is allowed in standard CMOS foundry. Because of this drawback, ISFET devices were primarily limited to research labs and were difficult to commercialize. Secondly, ISFET devices are relatively harder to scale down due to the large size. Even with a chip that has dimensions of a few millimeters, only a few ISFET devices can fit on a single chip (Kim et al. 2004). However, real-time recording of biological species require a large density of submicron scale sensor devices, along with real time read out circuits on chip (Shen et al. 2003). To circumvent the above hurdles, a unique CMOS-compatible sensor device architecture is proposed in this thesis.

2.2 Charge-Modulated Field Effect Transistor (CMFET)

To meet the goal of low cost and easy fabrication, CMOS-compatible sensor devices were recently proposed, and were called CvMOS and CMFET (Shen et al. 2003 and Barbaro et al. 2006). These two new sensor architectures inherit the merits of ISFET, and have their sensing gate capacitively coupled to the extended floating gate rather than exposing the gate directly to the elyctrolytes (Figure 3 and Figure 4). Additionally, ISFET devices are typically PMOS transistors if no extra electrode is to be added since the gate surface potential is around 0 volts (Kim et al. 2004). However, the new CvMOS and CMFET devices can be either NMOS or PMOS transistors as the sensing gate is capacitively coupled to the extended floating gate at the other side of transistor (Shen et al. 2003 and Barbaro et al. 2006). Interestingly, this control gate also makes the transistor's quiescent working point adjustable. By setting different control gate voltage, the transistor can always be tuned to certain static operation point to measure a varying signal.

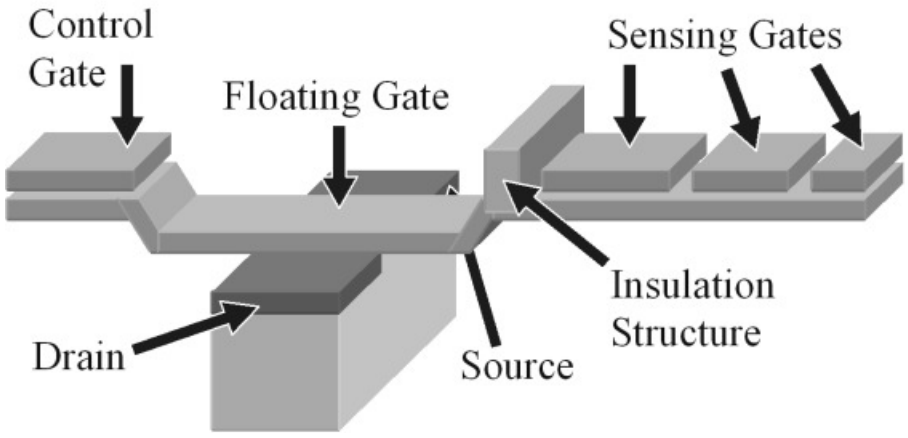

Figure 3. 3-D rendering of a CvMOS device structure with possible multiple sensing gates.

Extended floating gate FET devices were first introduced as vMOS, being constructed with multiple control gates capacitively coupled to the floating gate (Shibata et al. 1992). The floating gate voltage is established by summing the weighted input control gates voltages. From the inspiration of vMOS, CvMOS devices were designed by introducing proper dimensions of extra sensing gates, which could capture input information of electrostatic coupling from fluidic contacts.

In the first work on CvMOS devices, the n-channel MOSFET's width to length ratio was 2.5 (Figure 3) (Shen et al. 2003). Only one control gate was used, and several sensing gates were isolated and capactively coupled to the floating gate. Special preparation for the sensing gates to make microfluidic channel was also proposed for sensing areas. Two different CvMOS devices dimensions were presented, 4.8 μm × 356.8 μm and 76.8 μm × 356.8 μm. Original full-swing I-V curves were recorded for various kinds of fluid in the encapsulated channel on top of sensing area. Electrons then were tunneled onto and out of floating gate by apply ± 30V voltage, and a set of I-V curves were recorded with various sample fluids for the two cases. Analysis of the I-V curves reveal that the threshold voltage shifts in response to different fluids. The same experiments were repeated for meausring in the subthreshold region and transconductance measurements were performed. Their results were consistent and highly agreed on measuring the sensitivity of CvMOS device for sensing the fluids (Shen et al. 2003).

Shortly after CvMOS work, CMFET devices were presented as biomolecular process sensor in 2006. A model was built based on the extended floating gate transistor, with one control gate and one sensing gate (Figure 4). Physical model was built in a 3-D simulator, and the simulation results revealed a linear relationship of the floating gate voltage with the

charge on sensing gate. Compared to traditional sensors, CMFETs are very simple to fabricate as they are CMOS-compatible (with no complex additional process steps), straightforward in detection of DNA hybridization, and capable of being integrated into arrays with electronic readout (Barbaro et al. 2006).

Additionally, the authors demonstrated the use of CMFETs detect and study DNA hybridization (Barbaro et al. 2006). CMFET devices were fabricated with a sensing gate area ranging from 40μm × 40μm to 100μm × 100μm. In their experiments, the sensing gate was pre-coated with single-stranded DNA. Covalent immobilization took place once the complimentary ssDNA contained solution was dropped on the sensing gate. This subsequently changed charge on the sensing gate which were recorded as threshold voltage shifts compared to the reference devices (Barbaro et al. 2006).

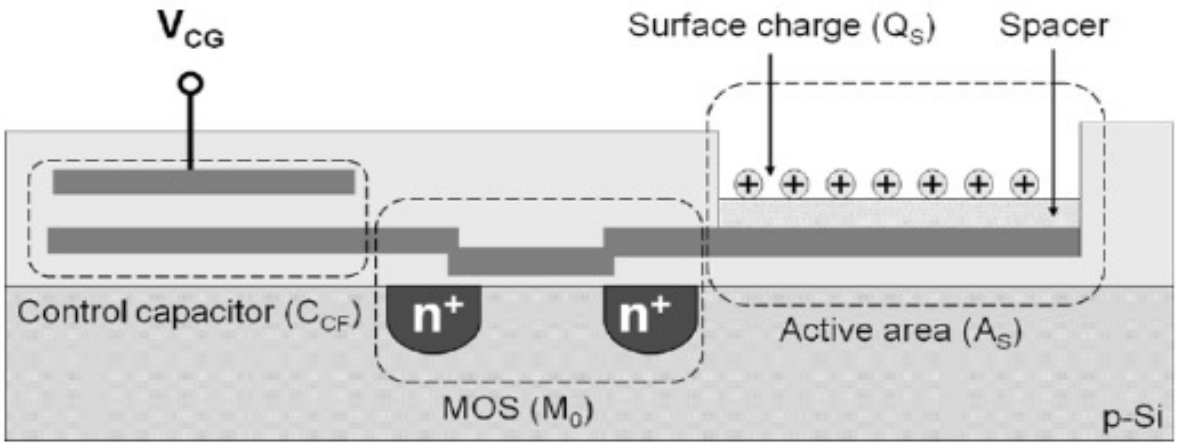

Figure 4. Cross sectional view of a CMFET device.

CvMOS and CMFET devices are attractive for their simple structure, relatively easy bioprocess detection, and highly feasible array implementation. However, as presented in

their published work, these devices are typically large in area (> 100 μm^2) and thus can't meet the needs of probing small scale biological species. Further more, the fabrication of CvMOS and CMFET devices require special post fabrication processes than can be complicated. Hence, new scalable and robust device designs for biosensing applications need to be explored.

2.3 Array implementation

For the application of large density array devices towards non-invasive, real time detection, highly sensitive and miniaturized electronic devices are needed with efficient signal readout and amplification. An example of the accompanying signal processor and circuitry is shown in the Figure 5 (Eversmann et al. 2003).

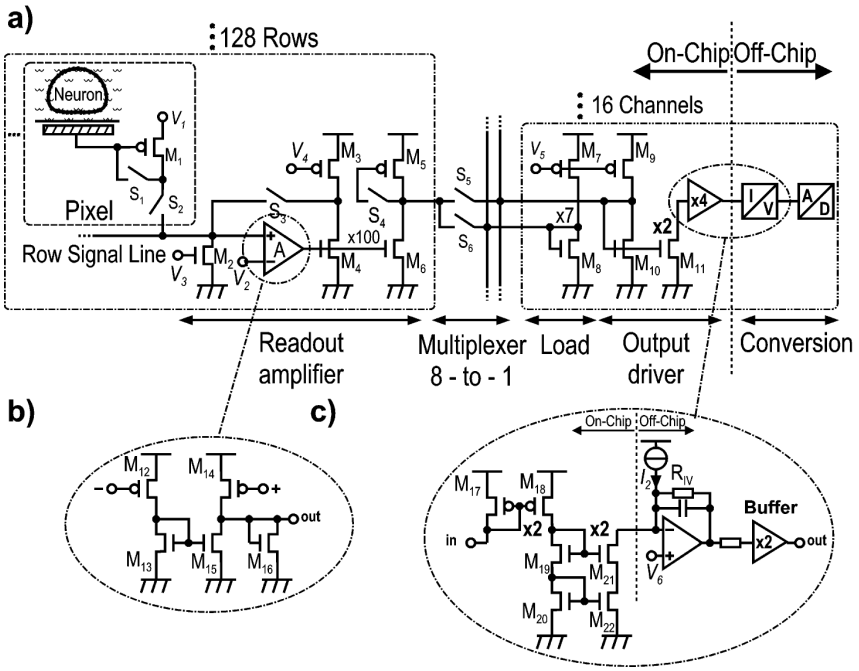

Figure 5. (a) Circuit diagram of the complete signal path. (b) Quasi-differential stage in readout amplifier. (c) Output driver and I/V conversion.

In 2003, a sophisticated biosensor array was realized for recording neurons activity. In their published report, a 128 x 128 pixels array was designed and fabricated in CMOS technology. Pixel circuits were formed by a PMOS transistor and two switches. The signals from pixel circuits were amplified to a proper value and read out through a multiplexer and as shown in Figure 5. Experiments were successfully done on recording the stimulated activities of neurons ([Eversmann et al. 2003]). Here, each pixel circuit uses a PMOS transistor as the sensing device, and quiescent working point is controlled by many extra transistors (Figure 5). The readout circuits were made very efficient and the area required for each pixel is kept small. The device works in deep saturation because that gate voltage is around the ground voltage, and this injects hot electrons into the floating gate, causing a shift of the threshold voltage. Complicated post layout processes (Figure 6) and several post layout steps were required before the chip is ready for use ([Eversmann et al. 2003]).

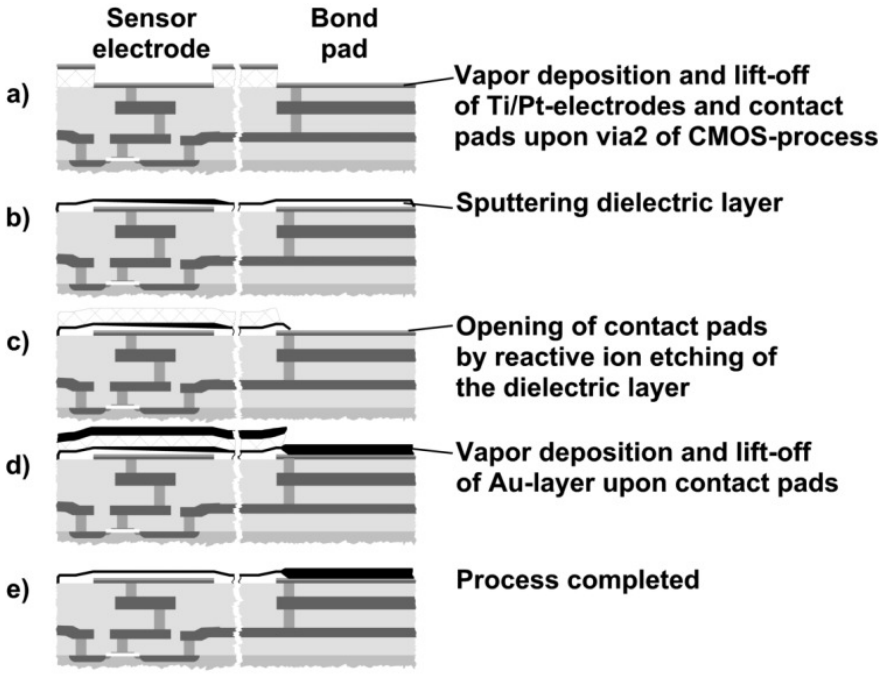

Figure 6. Schematic process flow for the array sensor.

In this thesis, we investigated new sensor device architectures that were a modified version of CMFET/CvMOS, with improved scaled down sizes for large array implementation and simplistic readout circuitry. The quiescent working point of our devices can be adjusted to avoid hot electrons injection, eliminating noise of the sensor. Also, in our design, the channel current can be directly read out instead of using numerous switches, amplifier and readout drive circuitry. The details of our proposed device and its workability will be discussed in the following chapters.

CHAPTER 3. MATERIALS AND METHODS

3.1 Charged poly electrolytes

Poly-L-Lysine and poly-L-Histidine are purchased from Fisher Scientific; poly Glutamic Acid and poly Aspartic Acid were purchased from Sigma-Aldrich. Poly Styrenesulfonic Acid Sodium Salt (PSASS), poly Allylamine Hydrochloride (PAHC), poly Diallyl Dimethyl Ammonium Chloride (PDDAC) and poly Acrylic Acid (PAA) are all purchased from Sigma-Aldrich. The designed Chips are submitted to the MOSIS foundry, fabricated in AMIS 1.5µm process, and packaged in DIP40.

3.2 Device model

The previous biosensor device model, CvMOS, was built as extended floating gate transistor whose input gates were capacitively coupled to the floating gate. Each input gate induces a voltage on the floating gate with weights determined by the ratio of the input gate capacitance to the total capacitance. The floating gate voltage is given by:

$$V_{FG} = \frac{Q}{C_T} + \frac{C_{gs}}{C_T} V_S + \frac{C_{gd}}{C_T} V_D + \sum_{j=1}^{N} \frac{C_j}{C_T} V_j \quad .$$

here Vj is the input voltage at jth input gate, C_T is the total capacitance, Q is the total static charge stored on floating gate, Cj is the capacitance of jth input gate (Shen et al. 2003).

After the published work on CvMOS, a different device architecture called the Charge-Modulated FET (CMFET) and shown in Figure 2 was reported in 2006. This device

had only one control gate and one sensing gate that was capacitively coupled to the extended floating gate. Similar to CvMOS, the floating gate voltage is given by :

$$V_{FG} = \frac{C_{CF}}{C_T} V_{CG} + \frac{Q_{F0} + Q_i}{C_T}.$$

where C_{CF} represents capacitance between control gate and floating gate, C_T is the total capacitance of the device. Q_{F0} is the total static charge stored on floating gate, and Q_i is the induced charge on sensing gate ([Barbaro et al. 2006]]).

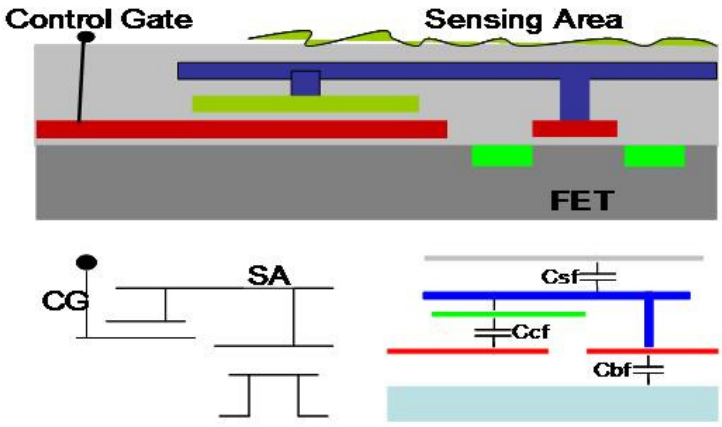

Figure 7. Cross sectional view, symbolic representation and capacitance model of our proposed Umbrella-Shaped Gate Field-Effect Transistor (UGFET).

Based on above two devices, we built our new biosensor device called Umbrella-shaped Gate FET (UGFET) and shown in Figure 7. Here, the sensing gate covers the entire device to maximize the sensing area and minimize the device size. To be compatible with standard CMOS fabrication process, the UGFET control gate is built using the first poly gate, which is underneath the floating gate made of second poly layer. The induced floating gate voltage therefore can be written in similar way:

$$V_{FG} = \frac{C_{CF}}{C_T} V_{CG} + \frac{Q_{F0} + Q_i}{C_T}.$$

In the above equation, the total capacitance includes three capacitances, C_{CF}, C_{SF}, and C_{BF}. Also, Q_{F0} is defined as the initial static charge. Since the amount of initial static charge is different from chip to chip, and the surface potential can fluctuate before and after immersing in DI water, the Q_{F0} is defined as the total static charge after the chip is rinsed with DI water. Q_i is the extra induced charge onto sensing area after charged biochemical solution was put onto the chip. With positive Q_i, the floating gate voltage increases with reference to DI water I-V curve. Hence, there will be less control voltage needed to turn on the UGFET device and so the I-V curve is shifted to the left of the reference I-V curve. Similarly, a negative Q_i is expected to shift the I-V curve to right of the reference curve.

3.3 Simulation and tests

UGFET devices are drawn and the layout is based on the AMIS 1.5μm technology library. Using this technology library in Cadence, the minimum size of device is obtained as 14.4μm×28.4μm after several design strategies. With the minimum size UGFET device information obtained, a 3-D model is built in Synopsys® Sentaurus Structure Device Editor. The simulation tool takes in device material parameters, then extracts all parasitics from the existing dimension and process, and outputs the distribution of carries, potentials and electric fields.

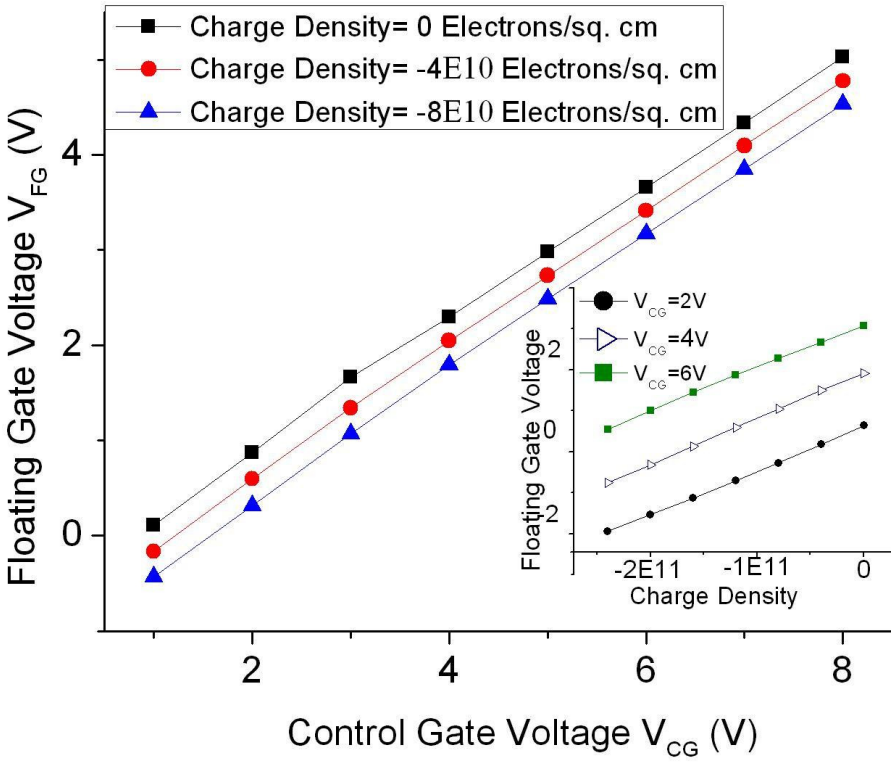

Figure 8. Floating gate voltage in response to control gate voltage, and floating gate voltage in response to charge density on sensing area.

With the Synopsys simulator, we were able to put miniscule charge onto the sensing area, and simulate the redistribution of potentials and charge fluctuation on the sensing area. Sweeping the control gate voltage from 0V to 8V, we see a linear dependence of the floating gate voltage on control gate voltage, as shown in Figure 8. The charge densities on sensing gate are 4×10^{10} electrons per square cm and 8×10^{10} electrons per square cm, and sensing gate is isolated from the floating gate by a 200 nm spacer. Figure 8 also shows the results of floating gate voltage versus the charge density on sensing gate. Sensing gate in this case is isolated from the floating gate by spacer of 30 nm. Three curves are plotted in Figure 8, with the control gate voltage of 2V, 4V and 6V separately; simulation results also show linear

dependence of floating gate voltage on the charge density on sensing gate. The simulation results further closely agree with the expression for the induced floating gate potential.

Our strategy of testing the UGFET devices is based on utilizing the fact that the I-V curves shift relative to a reference I-V curve. In our experiments, we used the I-V curve obtained with DI water exposed on the sensing area as the reference. We expect that during our charge sensing experiments, the I-V curves shift when exposed to biochemical solutions with reference to the DI water curves. Specifically, once biochemical solutions are dropped onto sensing area, the surface potential will be modified by the deposition of charged biomolecules. Modification of sensing gate surface potential will subsequently change the floating gate potential, and therefore shift the I-V curves of UGFET device. By measuring a set of I-V curves, and comparing with the DI water reference curve, the net polarity and amount of charge on sensing gate can be detected. The direction of the shift in the I-V curves and the amount of relative shifts will give us information about the charge polarity and charge density on the sensing area. Charge fluctuation during experimentation such as during DNA hybridization (Barbaro et al. 2006) thus be detected.

CHAPTER 4. UMBRELLA-SHAPED GATE FIELD-EFFECT TRANSISTOR

4.1 Layout and fabrication

In our first attempt, UGFET devices were laid out using AMIS 1.5µm technology library, with individual device sizes ranging from 14.4µm×28.4µm to 200µm×200µm. To our advantage, UGFET devices fully utilize the device size for sensing, and thus, its sensing gate size is same as the device size while the control gate is slightly smaller than sensing gate (Figure 7). Transistors for sensor devices are laid out as NMOS and gate width to length was kept as 3:1.

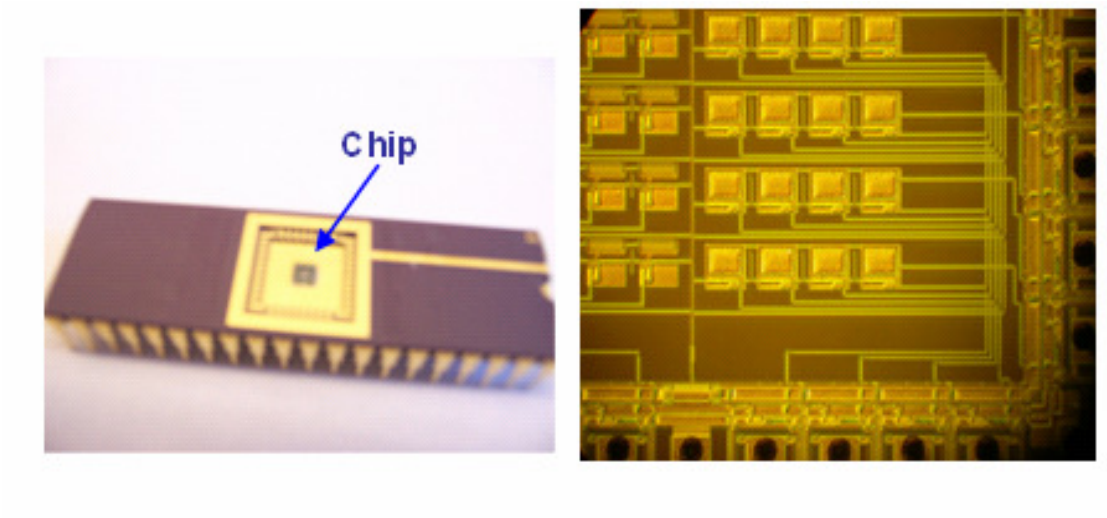

Figure 9. DIP40 packaged chip with 4×4 array implemented UGFET devices.

For comparison, two set of devices are laid out: one set with passivation openings on sensing gate and the other set of devices without any passivation openings (Appendix A). The passivation layer is put on top of sensing area after the entire chip is fabricated. This

passivation layer is around 500nm, but with opening on the sensing area, the passivation layer is cut which directly exposes the metal layer. The flexibility of having a opening in the passivation layer provides us a way to check if we need to decrease the sensing gate spacer to increase the experimental sensitivity. The drawn layout is submitted to MOSIS, fabricated in AMIS 1.5 μm process foundry, and packaged with 40-pin DIP. The packaged chips are shown in left side of Figure 9.

After successful testing of the individual UGFET devices, an array implemented chip is laid out with an array of 4 by 4 devices (Figure 9). To simplify the readout circuits, row control gates and column drains were connected to 4 pads separately. In this case, each control gate connected pad can select control gates in one specific row, and each drain connected pad can read out signals from drains in one specific column. So, during each time of the chip operation, only one row of devices are turned on by the "control pad", and only one column of the device drains are read out by the "drain pad". Therefore at any giving time, only one device is fully turned on and read out. This is similar to the way flash memory cells operate.

The latest generation of chips is 8 by 8 array, with row and column decoders to select and read out signals from each device in the array (Appendix A). Minimum sized UGFET devices were tightly packed into arrays to save the area (Figure 10). Similar to the previous 4 by 4 array, the row decoder determines the specific row of device to be turned on by applying a control gate voltage, and the column decoder select the column of devices to be read out.

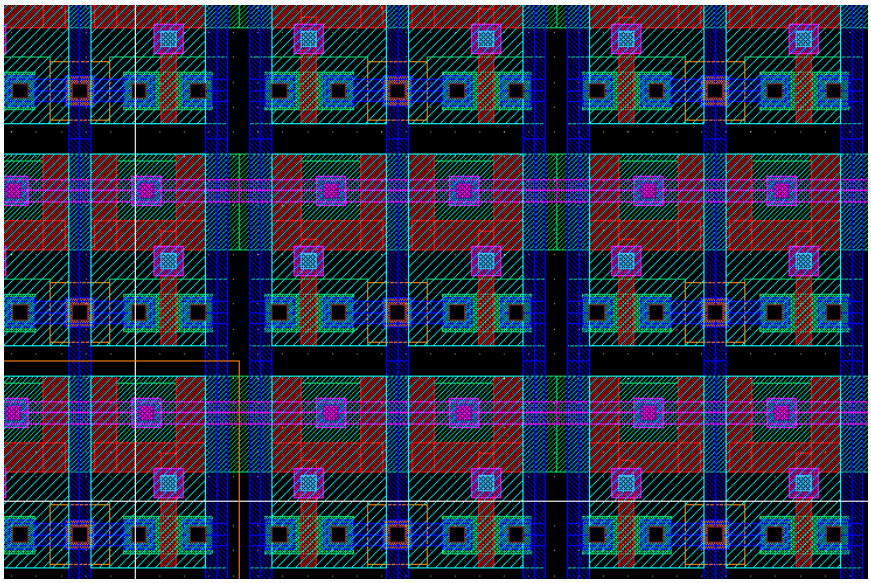

Figure 10. Layout of array of minimum sized UGFET.

4.2 Results

4.2.1 Testing preparation

The performance of any sensor device is judged based on its sensitivity, stability, and reproducibility. After the UGFET device chips were fabricated, the drain current versus control voltage and drain current versus drain voltage curves were recorded. Measurements were repeated several times on UGFEET devices of different sizes. A high consistency among all the measured curves was observed.

The fabricated devices were initially tested under dry conditions, during which the drain current versus control gate voltage at fixed drain voltage and drain current versus drain voltage at fixed control voltage were measured (Figure 11 and Figure 12). Judging from the characteristics of the plots, it is clear that the fabricated UGFET devices work well as

extended floating-gate field-effect transistors. The device is very sensitive to the voltage given to the control gate, and is consistant with the simulation results shown earlier.

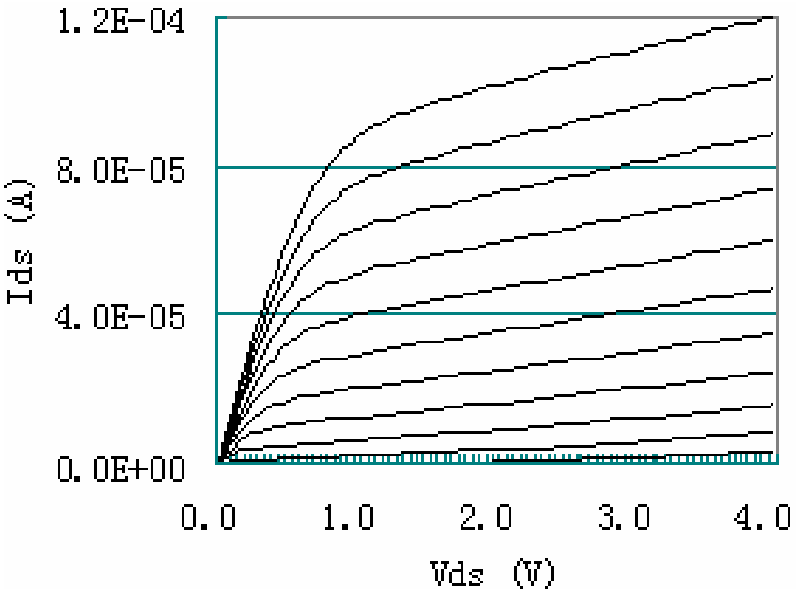

Figure 11. Drain current as a function of drain voltage at different control gate voltages.

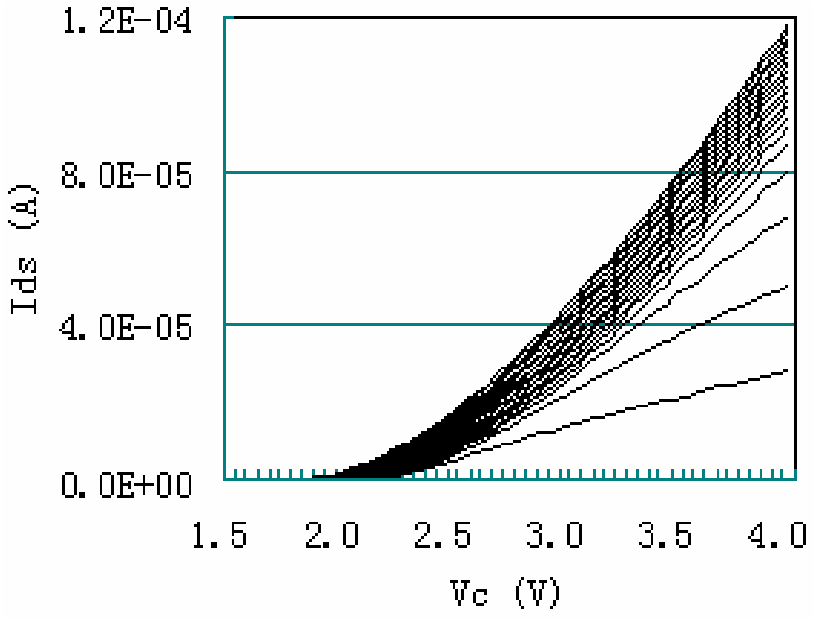

Figure 12. Drain current as a function of control gate voltage at different drain voltages.

These I-V results show that our UGFET devices are stable, and very sensitive to control voltage variations. As shown in the Figures 11 and 12, the applied voltage steps are only 0.2 volts, but the drain current difference is significant. This suggests that the UGFET will be very sensitive to the charges on sensing gate, since the floating gate voltage is delicately altered by control voltage as well as the sensing gate charge.

4.2.2 Threshold voltage technique

Measurements of the threshold voltage from the I-V curves is a well established method to determine the charges or carrier fluctuations over transistor. The relationship between drain current and control gate voltage for a transistor is given by:

$$I_{DS} = \beta * (V_{GS} - V_T)^2 * (1 - \lambda V_{DS}),$$

where I_{DS} is the current from drain to source, V_{GS} is the gate to source voltage, λ is the channel modulation parameter, and V_{DS} is the drain to source voltage. Plotting the derivative of I_{DS} versus V_{GS} and drawing a tangent at its curve from its peak value gives us threshold voltage. In our experiments, I-V curves were measured with biochemical solutions and compared with DI water.

The testing is started with DI water been dropped onto the chip carefully with a pipet. Each drop was about 1.2 μL with the help of accurately adjustable pipet. The DI water drop is centered on the chip to avoid contacting with any bonding wires and pads. This is needed to protect the wire connections and minimize the effects on sensing area potential. A group of I-V curves are measured for different DI water drops on the same chip. Here DI water was dropped onto chip, cleaned away after each measurement, and then another drop of DI water

was added again onto chip. The same processes are repeated after every test with biochemical solutions. As the results indicate, I-V curves keep shifting to right as the DI water rinsing goes on, but the shifting becomes more and more insignificant, and finally after 5 to 6 rounds of rinse, the shift is insignificant and negligible (Figure 13). This is the protocol we developed and followed, to achieve an unbiased reference point to compare with any new test results.

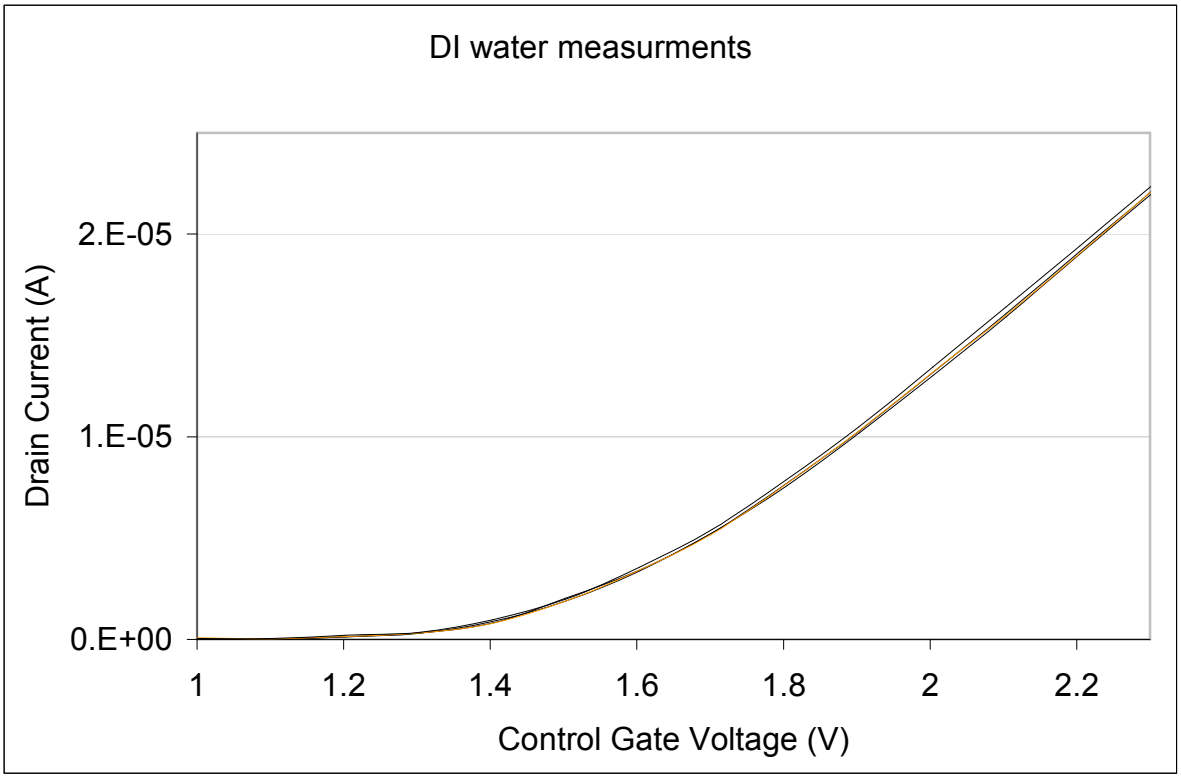

Figure 13. I-V measurements with DI water.

After the rinse with DI water, biochemical solutions are dropped onto the chip, covering the entire sensing area. This step needs to be more carefully done than dropping DI water because the biochemical solution is conductive, and contamination with bonding wires could eventually burn the wires. To be successful in this step, each time about 0.8 µL is

slowly injected through the pipet onto center of the chip. Measurements are taken for a discrete period of time after the solution is dropped onto the chip. From our observation, all experimental curves almost overlap each other, with little inherent noise. To further convince the reproducibility, test solutions are dropped onto chip surface, measurements are taken, and then the chip is rinsed with DI water several times to make sure I-V curve shift back to the reference curve. After the chip surface was dried, another drop of solution was then dropped onto chip, and measurements are taken again. The same steps are repeated numerous times and our results show consistent I-V curves for the same solution.

A set of I-V measurements for different biochemical solutions is then tested on chip. Figures 14 - 17 show the measured results for solutions with different types of charged poly amino acids. Compared to the reference, poly-L-Lysine and poly-Histidine solutions are positively charged, and they are considered to deposite positively charged layers which increases sensing area surface potential. From figures 14 and 15, shifts of I-V curves to left of the reference are detected. This measurement is consistent to our hypothesis that positively charged biomolecules will cause the I-V curves to shift to the left of the DI water reference curve.

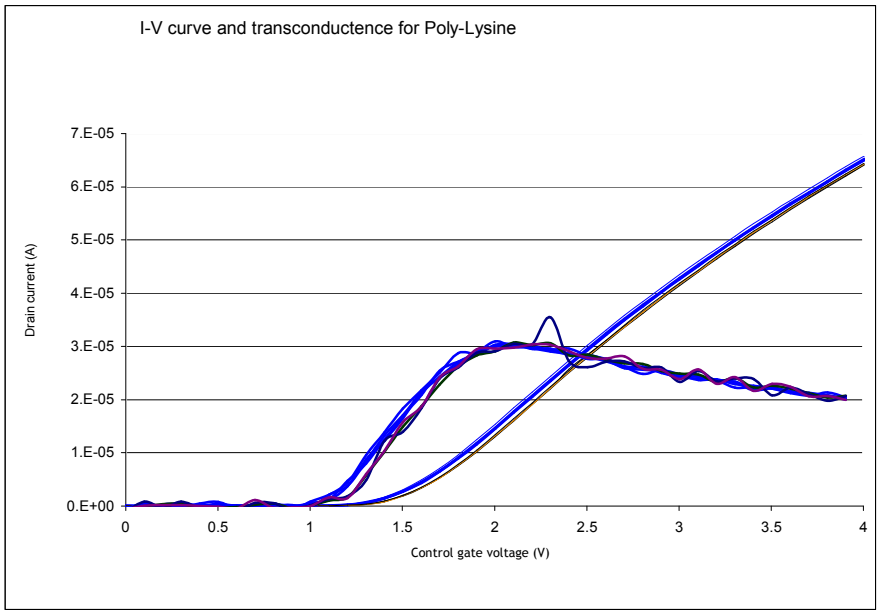

Figure 14. Drain current versus control gate voltage curves and their transconductance curves for poly-L-Lysine and DI water reference.

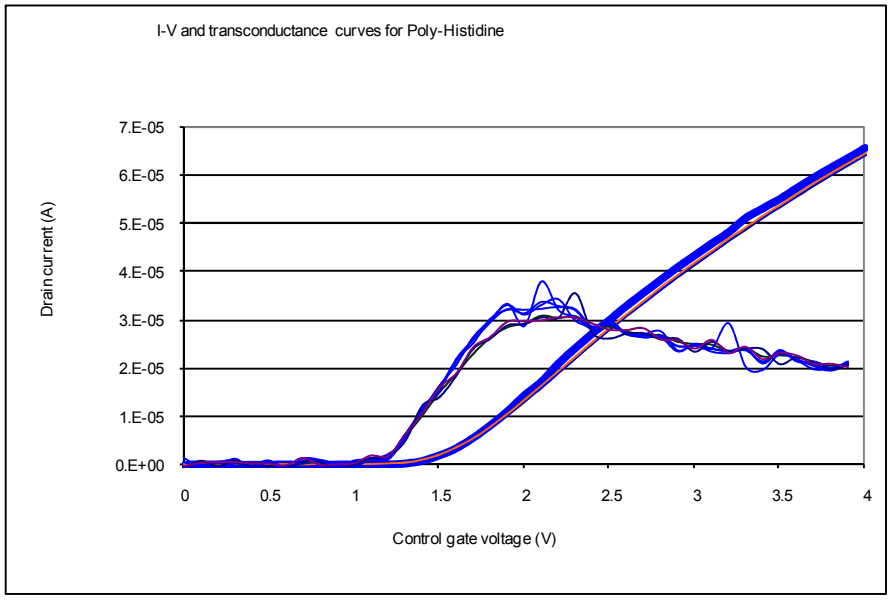

Figure 15. Drain current versus control gate voltage curves and their transconductance curves for poly-Histidine and DI water reference.

Poly-Aspartic acid and poly-Glutamic acid are negatively charged, and their solutions are expected to form a negatively charged deposition layer which will decrease sensing area surface potential. Again, the results in figures 16 and 17 show that shifts of I-V curves to right of the DI water reference, which is consistent with our hypothesis that positively charged biomolecules will cause the I-V curves to shift to the right of the DI water reference curves.

Threshold voltage is an important parameter to determine the shifts of I-V curves. Based on the well-established transconductance technique, threshold voltage can be obtained by transconductance plots. In figures 11 to 14, transconductance curves are plotted from the derivative of I-V curve, and threshold voltages are obtained by find the control gate voltage where the extension of linear part on transconductance curve crosses the control gate voltage axis. Threshold voltage shifts are revealed from different the poly amino acids. DI water I-V curve shows a threshold voltage of about 1.5V, while poly-L-Lysine and poly-Histerdine have a threshold voltage of about 1.4V. The threshold voltage for poly Asparatic Acid and poly Glutamic Acid are about 1.7V and 1.8V respectively. Poly-Glutamic Acid testing shows more shifting as shown in figure 4, because that Poly-Glutamic Acid is very hard to dissolve into water, so the grains in Poly Glutamic Acid suspension deposits onto sensing area of UGFET device, and make the surface charge density higher than Poly Asparatic Acid solution. Each measurement is repeated using the following procedure: 1. removing solution on chip, 2. rinsing with DI water several times while measuring the I-V curve until it almost shift back to DI water reference, 3. injecting another drop of solution. The repeated measurements show consistent shifts as expected, convincing us the repeatability and stability of detecting charges on the sensing gate of the our UGFET devices.

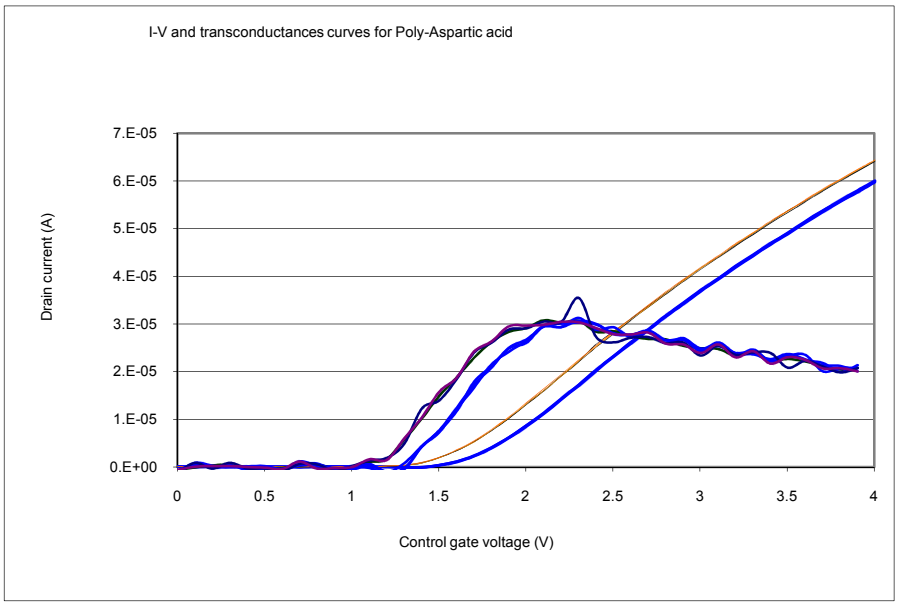

Figure 16. Drain current versus control gate voltage curves and their transconductance curves for poly-Aspartic acid and DI water reference.

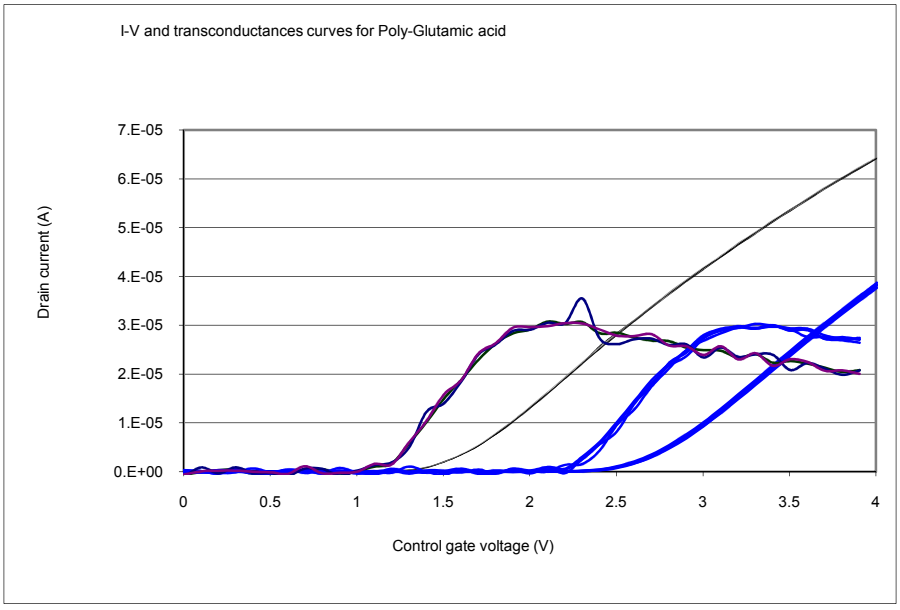

Figure 17. Drain current versus control gate voltage curves and their transconductance curves for poly-Glutamic acid and DI water reference.

As our testing results show, even without post layout processing, UGFET device with thick glass layer on sensing gate still demonstrates very good sensitivity. This is an advantage for UGFET devices, since the risk of introduce more static charges onto device by post layout processing is absent. This also avoids damage of device functionality, ensuring high yield of individual devices and significantly ensuring the over all yield of the implemented device array.

4.2.3 Subthreshold slope technique

Another technique developed for detecting charges on the sensing gate of UGFET devices is the subthreshold voltage method. Instead of measuring curves of drain current versus control voltage, curves of drain current versus gate voltage is measured while keeping the transistor in the subthreshold region.

A group of Poly Acrylic Acid (PAA) solutions of different concentrations are tested on chip. After each measurement, DI water is used to rinse the chip surface. As shown in Figure 18, all reference curves for DI water rinsing after each solution are overlapping, which makes sure that the surface is rinsed clean enough. Measured curves show a consistent shift to left with the increasing of solution concentration. These results are as expected since increasing the solution concentration deposits more charged biomolecules onto the sensing area surface, and thereby increases surface potential.

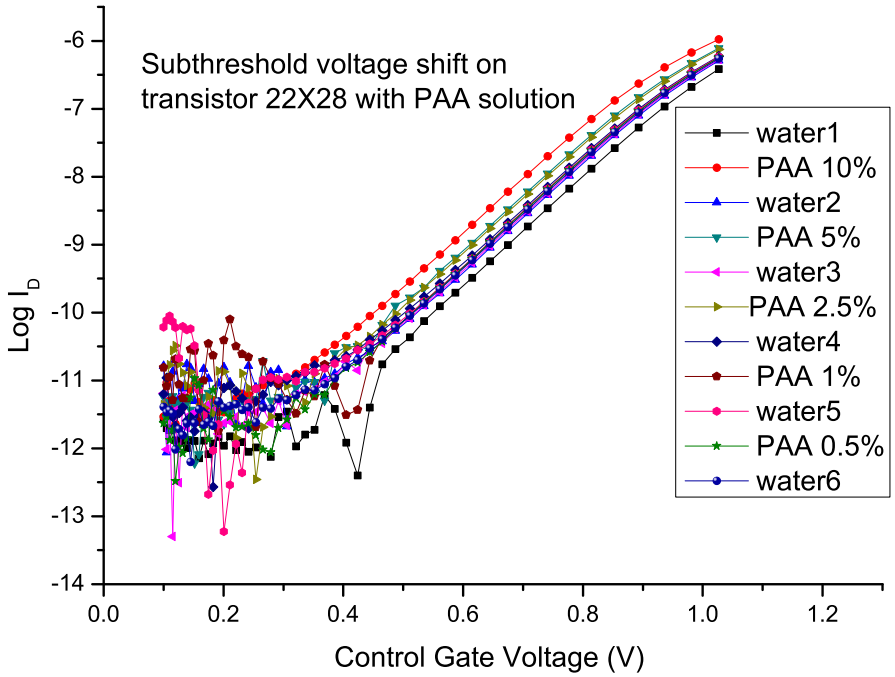

Figure 18. Drain current in log scale versus control gate voltage.

Several other solutions are tested on chip, the results are analyzed, and relative subthreshold voltage shifts derived from the measurements are plotted in Figure 19. Poly Styrenesulfonic Acid Sodium Salt (PSASS), Poly Allylamine Hydrochloride (PAHC) and Poly Diallyl Dimethyl Ammonium Chloride (PDDAC) are tested using the same protocol as used for PAA. A set of curves of drain current versus drain voltage are recorded, their relative subthreshold voltage shifts are determined for corresponding solution concentrations. From figure 19, a steadily increasing subthreshold voltage shifts with increasing solution concentration is measured for all charged polyelectrolytes' solutions.

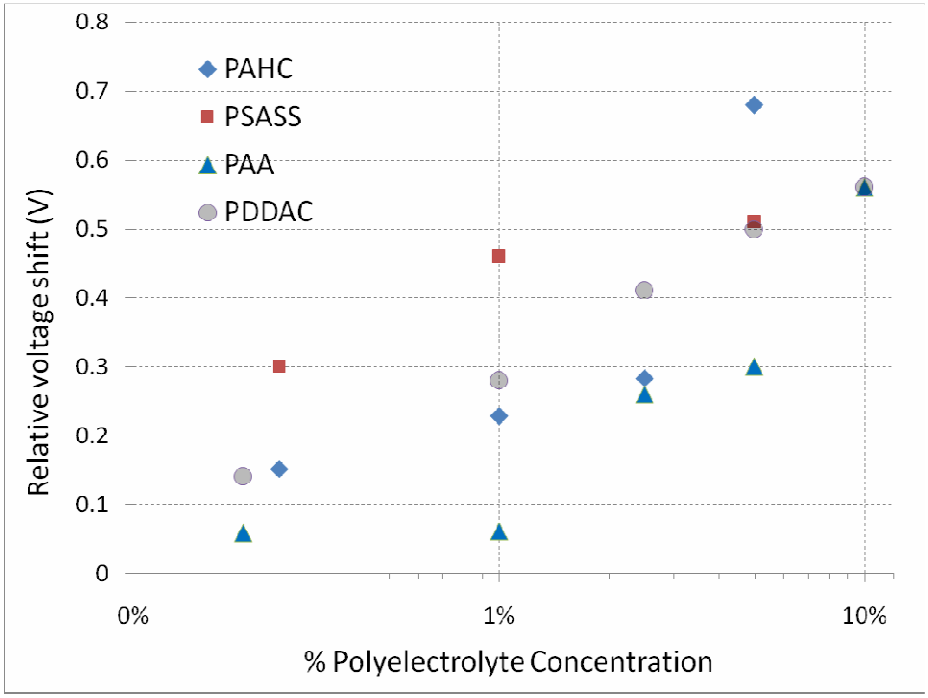

Figure 19. Relative subthreshold voltage shifts versus the charged poly amino acids concentration for PAHC, PSASS, PAA and PDDAC.

4.2.4 Array implementations

UGFET devices are also implemented into an array of 8 by 8 devices, with row and column decoders to select one particular device each time. With the programmed HP Semiconductor Parameter Analyzer 4145, the whole array is tested rapidly. Repeated testing of the array chip reveals the individual device functionality has not been compromised in the array implementation. Possible applications for testing biological species such as neurons are under way. The cell growth medium is a necessary solution for growing neurons on chip, and testing with a fixed concentration growth medium solution has shown stable I-V curves for our UGFET devices.

Cell detection and monitoring requires a high density of sensor devices with least amount of small blank space between individual sensing devices. Exciting applications such as monitering neurons' activity with high density sensor array has been proposed recently and we are using the same methodology on our UGFET sensor array (Eversmann et al. 2003). Work is being pursued for applications such as cell detection and real time monitoring of cell activity. Each designed UGFET sensor is considerably smaller than an individual cell, and has minimal "blind" space between each device sensing area. Furthermore, our UGFET device can be scaled down much smaller by fabricating in advanced submicron process, while keeping the "blind" area very small compared to the device size. All these merits indicate high potential of UGFET device array for real time detection, non-destructive sensing, and characterization of biological processes.

CHAPTER 5. CONCLUSION

5.1 Conclusion

Previous research on Charge-Modulated FET (CMFET) devices have shown good sensitivity, stability and CMOS compatibility, but their extended floating gate design makes it ineffective in scalability and high density implementation for VLSI applications ([Barbaro et al. 2006] and [Shen et al. 2003]). Our charge modulated UGFET sensor devices, adopted the merits of previous designs, and effectively modified their architecture to minimize the device size while maximizing the sensing area. In our novel design, the sensing gate covers the entire device area, and saves on extra lateral space need for extended floating gate.

The UGFET device simulations confirm its sensitivity and stability while the device testing further proves its reliability. Drain current versus control gate voltage curves are obtained from UGFET devices exposed to a set of poly amino acids. The test results show that positively charged poly Lysine and poly Histidine curves shift to the left of DI water reference plot, with approximately a negative shift of 0.1 volts. The negatively charged poly Aspartic acid and poly Glutamic acid I-V curves shift to the right of DI water reference plot, with positive shift of approximately 0.2 to 0.3 volts.

Drain current versus drain to source voltage are recorded for several polyelectrolytes of varying concentrations. Subthreshold slops also were derived from the measured I-V curves. Results showed that the shifts keep increasing with increasing concentration, which is due to the increased deposition of charged electrolytes onto the surface of sensing area.

UGFET devices are also implemented into a chip with of 8 by 8 array. Each device in the array is accessed individually at one time by the selection of row and column decoders.

Devices in the array are also tested in same procedure as individual device testing. Our test results reaffirm the high sensitivity and scalability of our sensor devices and their application as high density array chips in detecting and recording biological species, such as neurons ([Eversmann et al. 2003]).

5.2 Future work

The designed UGFET sensor array chip can be used to detect biological specimens such as cells, protein and DNA. Lab-on-chip possible applications include building lab-on-chip systems for cell detection and electric physical recording. In our experiments, we have shown the possibility of putting live cell onto UGFET sensor chips and recording their activities (Appendix B). Biological and chemical testing is underway, which could lead to real time detection and monitoring of biochemical specimens. With available submicron fabrication processes, much smaller sensor devices can be realized, thereby significantly improving the experimental resolution of detection can be achieved.

APPENDIX A. LAYOUT OF UGFET DEVICES

The layout of Individual UGFET devices with various sizes were drawn on first chip. For better comparison, the devices are divided into two groups, one with openings, and the other group without openings (Figure A.1).

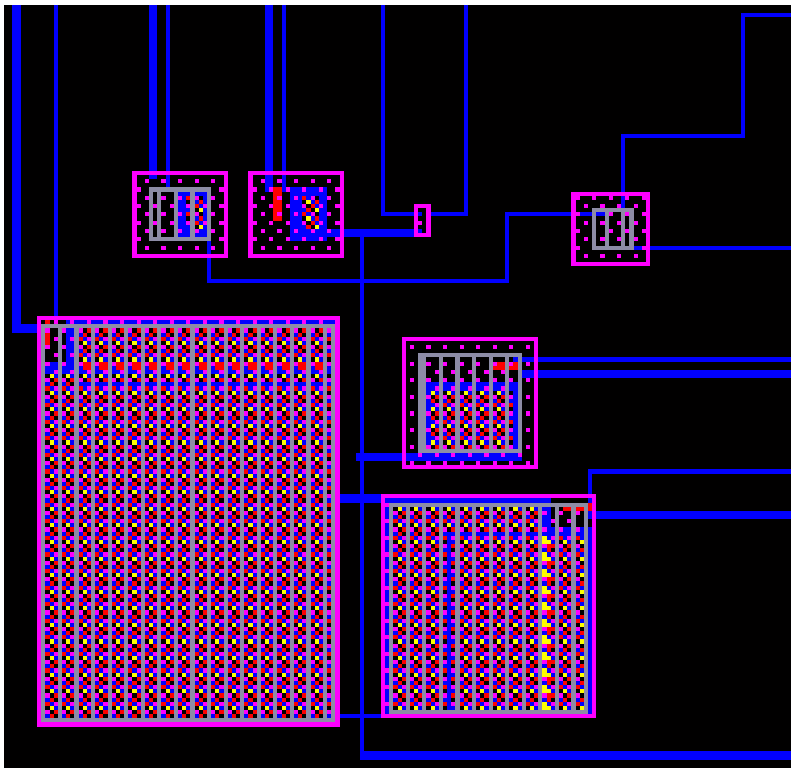

Figure A.1: Layout of individual devices with different size.

The whole view of first chip is shown in Figure A.2, of which the right top section is for UGFET devices (shown in Figure A.1).

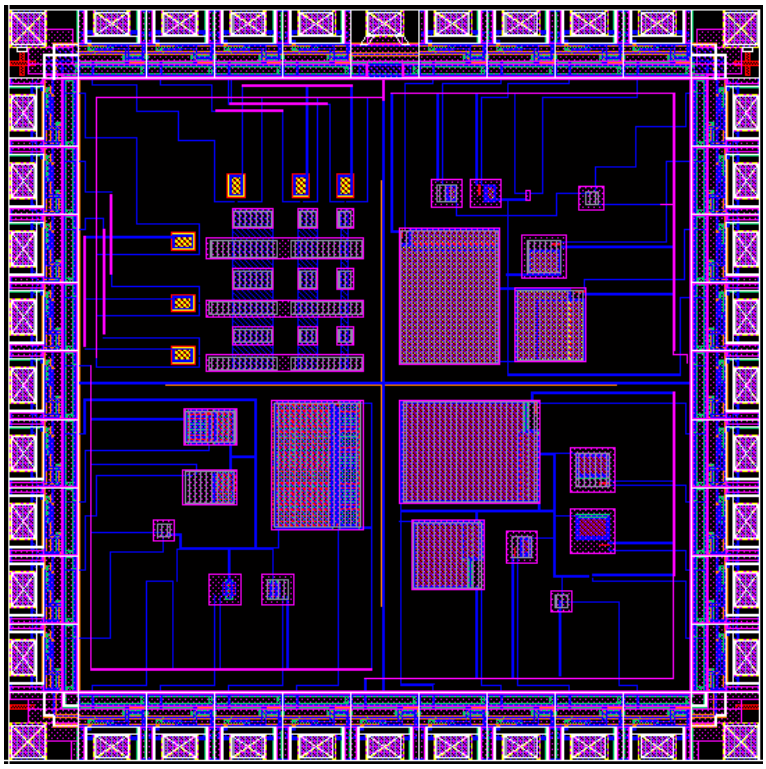

Figure A.2: Whole view of sensor devices chip using our first design.

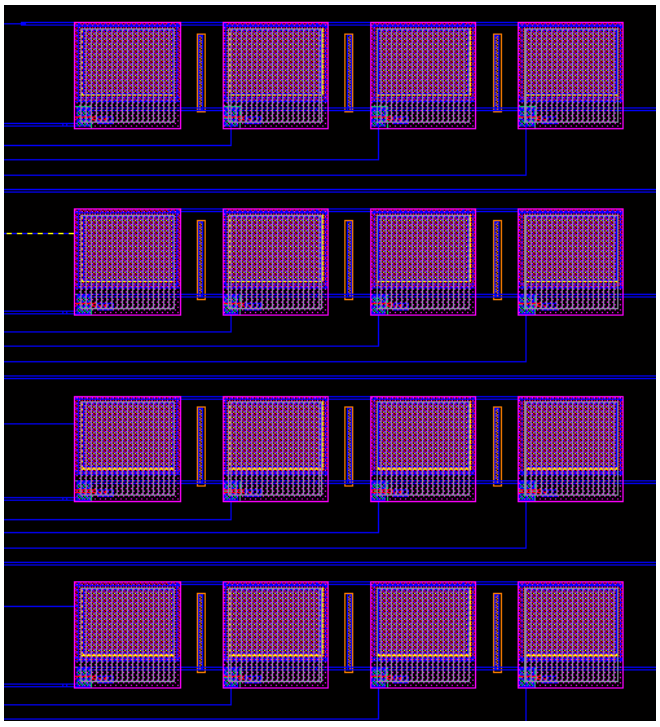

Figure A.3: 4×4 array of UGFET.

Figure A.3 shows an array implementation of a 4×4 array of UGFET devices. Each row is selected by a control gate voltage pad, while each column is read by a drain current read out pad. Figure A.4 shows the sensor devices connected in an array.

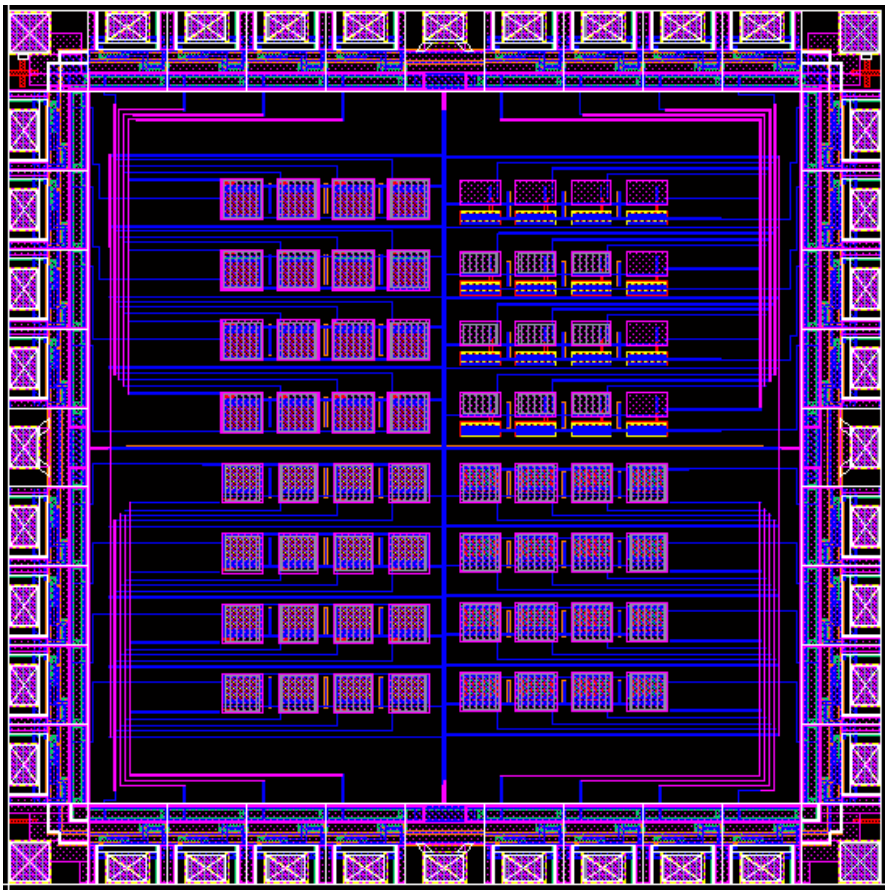

Figure A.4: Whole view of second array implemented devices chip.

Figure A.5 shows an 8×8 array implemented UGFET devices with row and column decoders. The array was shown at left bottom part of the figure. Only 3 pads were used to specifically for 8 rows and 8 columns, which saves 5 pads in each case compared to the 4×4 array chip.

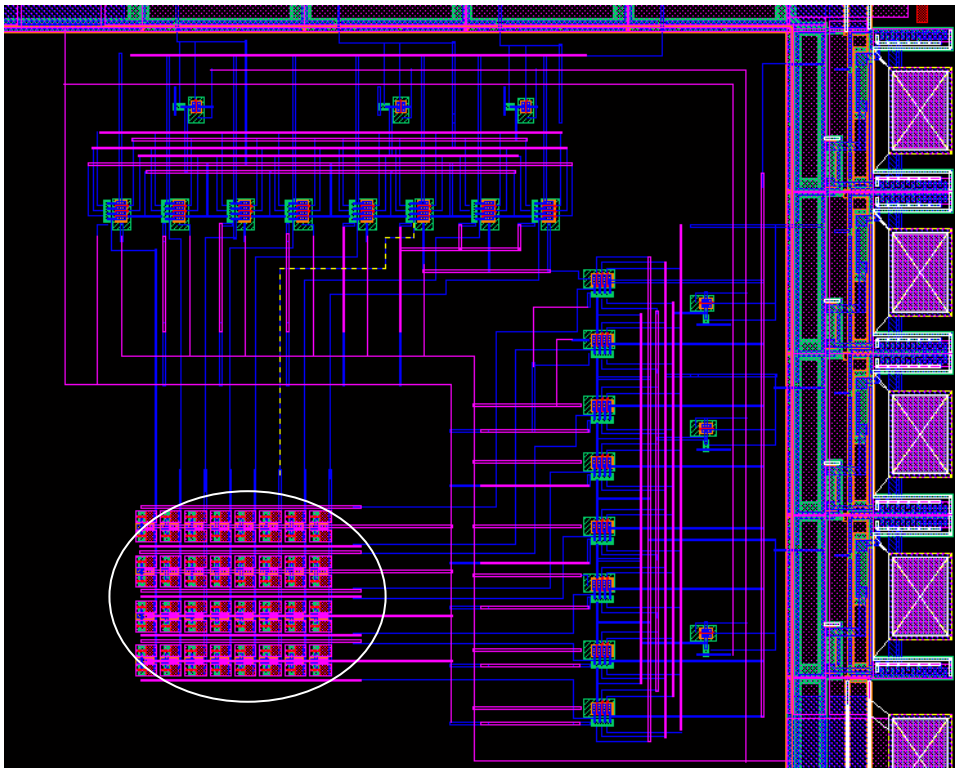

Figure A.5: 8×8 array implemented UGFET with row and column decoders. The Array of device is highlighted in the circle.

APPENDIX B. TESTING WITH CHO CELLS

CHO cells were put on chip for testing. In Figure B.1, two cells were located on top of sensor device.

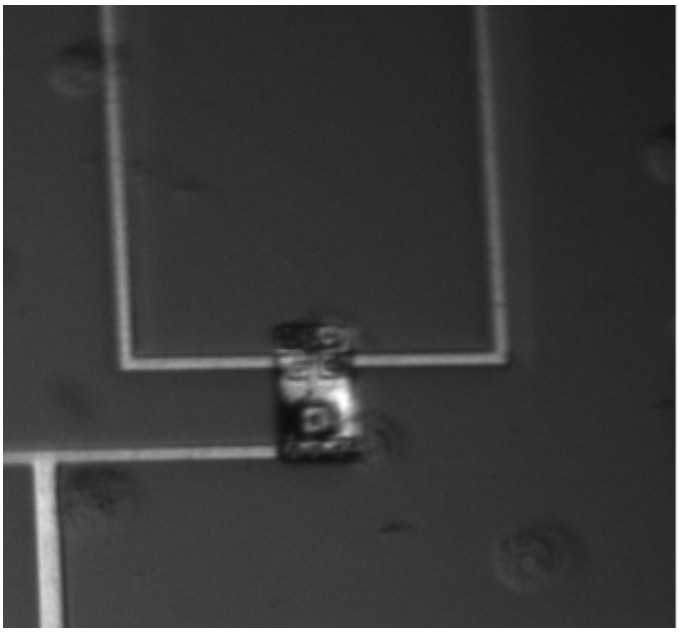

Figure B.1: CHO cells test with UGFET devices.

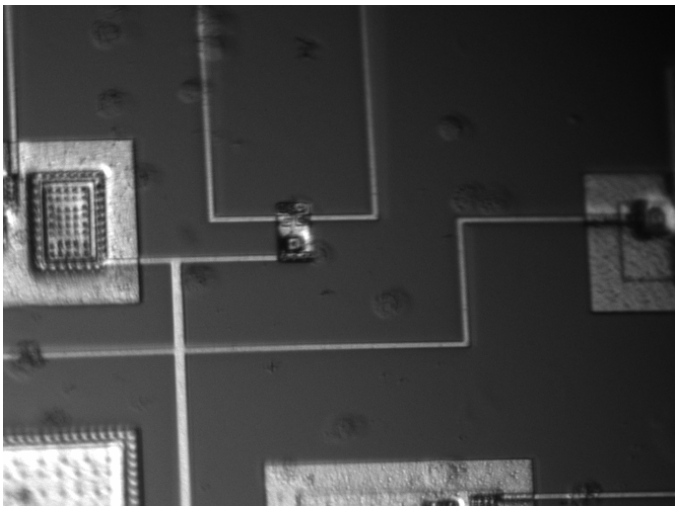

Figure B.2: Lager view of CHO cells testing with UGFET devices.

BIBLIOGRAPHY

(1) Pedano M.L., Rivas G.A., 2003. Biosensors and Bioelectronics 18(2-3), 269-277.

(2) Kim Y., Jeong Y., Park H., Shin J., Choi P., Lim G., 2004. Biosensors and Bioelectronics 20(1), 69-74.

(3) Chiti G., Marrazza G., Mascini M., 2001. Anal. Chim. Acta 427(2), 155-164.

(4) Schoning M.J., Poghossian A., 2006. Electroanalysis 18(19-20), 1893-1900.

(5) Lehmann M., Baumann W., Brischwein M., et al., 2001. Biosensors & Bioelectronics 16(3), 195-203.

(6) Kim D., Jeong Y., et al., 2004. Biosensors & Bioelectronics 20(1), 69-74.

(7) Bergveld P., 1970. IEEE Trans. Biomed. Eng. 17, pages 70-71.

(8) Barbaro M., Bonfiglio A., Raffo L., Alessandrini A., et al., 2006. Electron Device Letters, IEEE 27 (7), 595-597.

(9) Dzyadevych S.V., Soldatkin A.P., El'skaya A.V., et al., 2006. Analytica Chimica Acta 568, 248-58.

(10) Truman P., Uhlmann P., Stamm M., 2006. Lab Chip 6, 1220-1228.

(11) Shibata T., Ohmi T., 1992. IEEE Trans. Electron Devices 39, 1444-1455.

(12) Barbaro M., Bonfiglio A., Raffo L., 2006. *IEEE* Trans. Electron Devices 53, 158-166.

(13) Shen N., Liu Z., Lee C., Minch B., Kan E., 2003. IEEE Trans. Electron Devices 50(10), 2171-2178.

(14) Eversmann B., Jenkner M., Hofmann F., Paulus C., et al., 2003. IEEE J. Solid-State Circuits 38(12), 2306-2317.

ACKNOWLEDGEMENT

I would like to express my gratitude to everyone who helped me at different junctions at this research. First and foremost, Dr. Pandey for his guidance, patience and support throughout my research and the writing of this thesis. His insights and words of encouragement have often inspired me and renewed my hopes for completing the project. I would also like to thank my committee members for their efforts and contributions to this work: Dr. Dong and Dr. Yu. I would additionally like to thank Pam Meyers for her administrative help and support. Last but not the least, my colleague friendly, Baozhen Chen for his intellectual and technical support.